Environ. Sci. Technol. **2009,** *43,* 8573–8579

Hemispheres-in-Cell Geometry to Predict Colloid Deposition in Porous Media

HUILIAN MA,[†] JULIEN PEDEL,[‡] PAUL FIFE,[§] AND WILLIAM P. JOHNSON*,[†]

Department of Geology and Geophysics, Department of Chemical Engineering, and Department of Mathematics, University of Utah, Salt Lake City, Utah 84112

Received April 27, 2009. Revised manuscript received September 23, 2009. Accepted September 25, 2009.

A "hemispheres-in-cell" geometry is provided for prediction of colloid retention during transport in porous media. This new geometry preserves the utilities provided in the Happel sphere-in-cell geometry; namely, the ability to predict deposition for a range of porosities, and representation of the influence of neighboring collectors on the fluid flow field. The new geometry, which includes grain to grain contact, is justified by the eventual goal of predicting colloid deposition in the presence of energy barriers, which has been shown in previous literature to involve deposition within grain to grain contacts for colloid: collector ratios greater than approximately 0.005. In order to serve as a platform for predicting deposition in the presence of energy barriers, the model must be shown capable of quantitatively predicting deposition in the absence of energy barriers, which is a requirement that was not met by previous grain to grain contact geometries. This paper describes development of the fluid flow field and particle trajectory simulations for the hemispheres-in-cell geometry in the absence of energy barriers, and demonstrates that the resulting simulations compare favorably to existing models and experiments. A correlation equation for predicting collector efficiencies in the hemispheres-in-cell model in the absence of energy barriers was developed via regression of numerical results to dimensionless parameters.

Introduction

No mechanistic colloid transport theory yet exists to predict colloidal deposition in the environment, where repulsion typically exists between colloids and porous media grain surfaces, despite the fact that the transport and deposition of colloidal particles in saturated porous media is essential to various environmental processes including riverbank filtration, prediction of pathogen transport distances from septic systems, and colloid-facilitated contaminant transport.

The theoretical framework commonly used to predict colloid transport and deposition in porous media is classic colloid filtration theory (CFT) (*1–4*). CFT describes fluid flow and colloid transport in porous media based on the Happel sphere-in-cell model (*5*), which represents porous media via a solid sphere encircled by a spherical fluid shell, where the thickness of the fluid shell is chosen such that the porosity of this unit cell is equal to the actual porosity of a packed bed. The probability of colloid interception and retention in this cell is determined through particle trajectory (or flux) simulations, which are based on a mechanistic force and torque balance on the colloid within the flow field of the unit cell; wherein, for the particle trajectory approach, the forces are assessed, the colloid is translated accordingly, and the process repeated until the colloid either exits, or is retained within the cell (*1–3*). These mechanistic numerical simulations yield the number of colloids that intercept the collector relative to the number of colloids that enter the unit cell, which is the so-called collector efficiency (η). The values of η determined under a range of conditions (e.g., variety of porosities, colloid sizes) have been regressed to dimensionless parameters to provide correlation equations for estimation of η (*2, 3*). CFT serves as an excellent predictive tool for colloid retention in simple porous media; but only when energy barriers to deposition are absent (favorable conditions) (*6–8*). When energy barriers to deposition are present (unfavorable conditions), the mechanistic numerical simulations predict that no deposition will occur. The mechanistic simulations underlying CFT indicate that colloids can overcome energy barriers only when the barriers are very small, e.g., $< \sim 10\ kT$, where k is the Boltzmann constant and T is the absolute temperature.

To develop mechanistic predictors of retention in the presence of energy barriers, the essential mechanisms of colloid retention must be identified and incorporated. Experiments indicate that places where colloid retention is possible include: (i) "Holes" in the energy barrier where the energy barrier is reduced or eliminated via surface roughness or heterogeneity (e.g., heterodomains of attractive charge) (*9, 10*). (ii) Grain-to-grain contacts where colloids may be wedged between energy barriers and push through one of them into contact with the surface (*11, 12*), or straining, which is not clearly defined, but which conceptually involves grain-to-grain contacts (*13*). (iii) Zones of low fluid drag where secondary energy minimum—associated colloids may be retained without attachment (*8, 14, 15*).

Colloid retention in the presence of energy barriers by the above mechanisms has been demonstrated in mechanistic simulations in unit cells containing multiple grains in various packing arrangements (*11, 16*). These simulations corroborate expectations from experiments; however, to serve as a predictive framework, mechanistic simulations should provide good prediction in both the absence and presence of energy barriers. Unfortunately, the packing arrangements examined to date predict collector efficiencies in the absence of energy barriers that are far higher than those predicted by existing theory, as well as those determined from experiments (*11*). Furthermore, to serve as a predictive framework, these unit cells need to be capable of representing the spectrum of porosities encountered in environmental systems. The fixed porosities of the unit cells (e.g., 0.26 for dense cubic packing and 0.476 for simple cubic packing) limit their suitability to represent a range of porosities.

The foundation for a general colloid filtration theory (for prediction in both the absence and presence of energy barriers) needs to meet at minimum the following three criteria: (1) able to represent a range of porosities; (2) provide accurate prediction of η in the absence of energy barriers; (3) incorporate attributes to allow colloid retention in the presence of energy barriers (e.g., grain-to-grain contacts). The Happel sphere-in-cell model provides an elegant tem-

* Corresponding author phone: (801)585-5033; fax: (801)581-7065; e-mail: william.johnson@utah.edu.
[†] Department of Geology and Geophysics.
[‡] Department of Chemical Engineering.
[§] Department of Mathematics.

10.1021/es901242b CCC: $40.75
Published on Web 10/12/2009

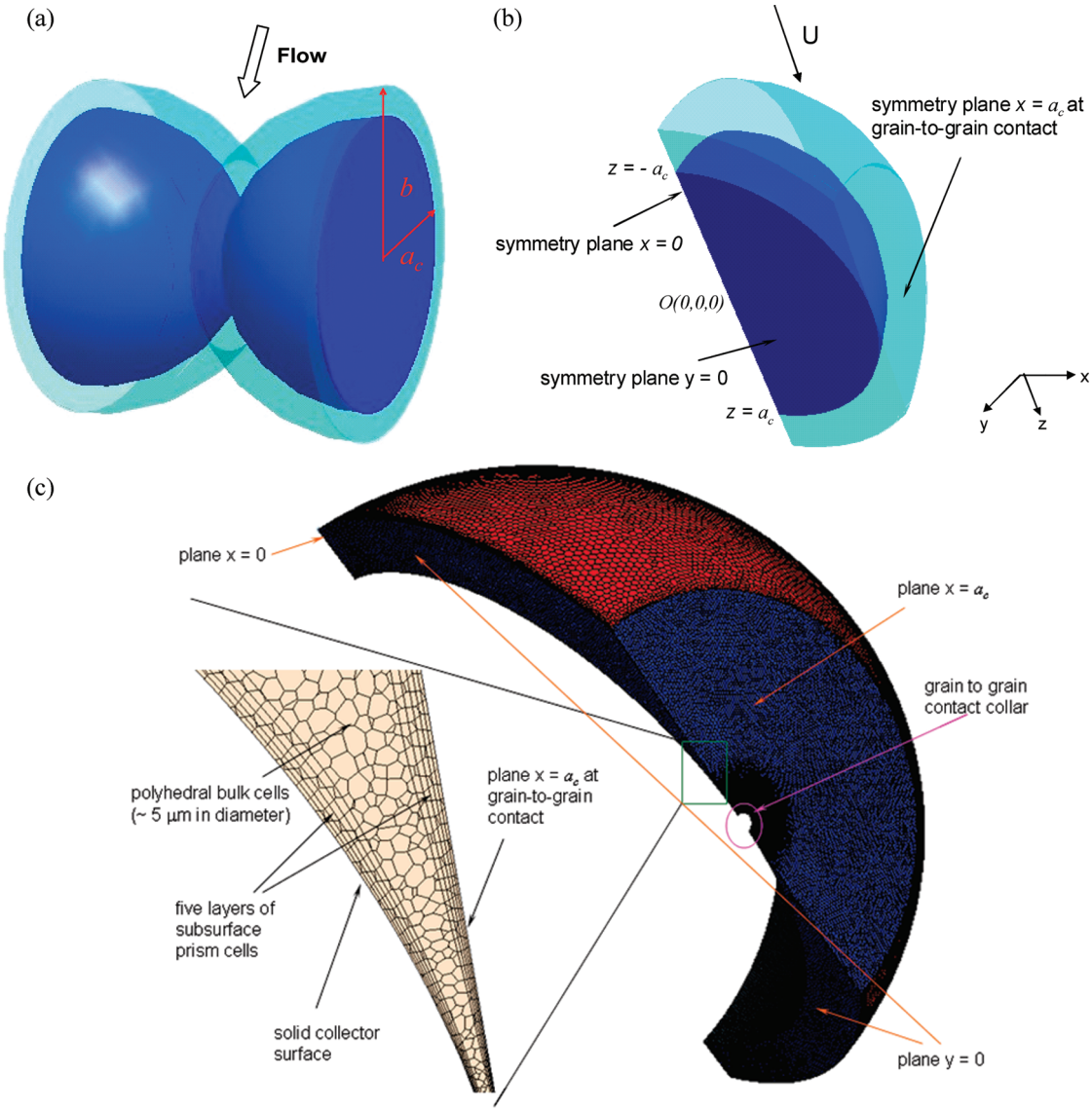

FIGURE 1. (a) The hemispheres-in-cell model geometry contains a grain-to-grain contact and can represent a spectrum of porosities by varying the fluid shell (light sea green) thickness ($b - a_c$) relative to the collector (blue) radius (a_c). The flow is directed perpendicular to the line connecting the two-hemisphere centers. (b) The quadrant of the hemispheres-in-cell model confined between ($x \in (0, a_c)$, $y \in (-b, 0)$) with all the symmetry planes ($x = 0$, $x = a_c$, and $y = 0$) shown; the positions of forward and rear stagnation points were indicated by $z = -a_c$ and $z = a_c$, respectively. (c) An image of representative computational meshes constructed for (b), with the inset showing an image of meshes close to the grain-to-grain contact.

plate not only because it is able to represent various porosities, but also because the flow field surrounding the solid grain is enveloped within an outer boundary that represents the "divide" separating the influences of adjacent grains in the flow field (achieved via zero radial velocity and zero non-tangential stress conditions at this boundary). To achieve these physically meaningful boundaries, the Happel sphere-in-cell model is geometrically nonphysical, meaning that the Happel unit cells are not "stackable", i.e., one cannot assemble a meaningful porous medium by assembling multiple Happel unit cells. However, the unit cells have known volume, allowing determination of the number of unit cells corresponding to a known volume of porous media. By incorporating these features, the Happel sphere-in-cell model captures the relevant processes in fluid flow and particle transport in porous media in the absence of energy barriers, as demonstrated by its excellent predictive capability under these conditions.

For the purpose of developing predictive capability in both the absence and presence of energy barriers, we propose a new unit cell (the hemispheres-in-cell model), which preserves the utilities provided in the Happel sphere-in-cell model, but which incorporates features (i.e., grain-to-grain contact) that potentially allow colloid retention in the presence of energy barriers. The purpose of this paper is to demonstrate the performance of the hemispheres-in-cell model under favorable conditions (in the absence of energy barriers to deposition), e.g., its accuracy of prediction relative to existing theory.

Model Development

Numerical Analysis of Fluid Flow. Like the Happel sphere-in-cell model, the Hemispheres-in-cell model represents a spectrum of porosities in porous media by varying the outer fluid envelope radius (b) relative to the collector radius (a_c) (Figure 1a). Unlike the Happel sphere-in-cell model, the Hemispheres-in-cell model incorporates a grain-to-grain contact, which complicates obtaining an accurate fluid flow field proximal and distal to the grain surface. The lack of availability of closed-form solutions for the fluid flow field in the hemispheres-in-cell model (see Supporting Information (SI) for more details) requires derivation of the flow field

TABLE 1. Lagrangian Trajectory Simulation Parameters

parameter	value
collector diameter, d_c	510 μm
porosity, ε	0.37
approach velocity, U	1.48 m/day
particle density, ρ_p	1055 kg/m^3
fluid density, ρ_f	998 kg/m^3
fluid viscosity, μ	9.98×10^{-4} kg·m/s
Hamaker constant, H	3.84×10^{-21} J
absolute temperature, T	298.2 K
time step, Δt	10 MRT[a] (lower limit)

[a] MRT refers to the particle momentum relaxation time.

using computational fluid dynamics, as was done here using STAR-CD and Star-ccm+ (*17*), with meshes constructed under guidelines ensuring convergence and stability (see SI). Because of symmetry on the $x = a_c$ and $y = 0$ planes, mesh simulations were required only for one quadrant; e.g., the quadrant defined by ($x \in (0, a_c)$, $y \in (-b, 0)$) of the hemispheres-in-cell model (Figure 1b) was composed of ~1.06 million cells (Figure 1c), for the case where $\varepsilon = 0.37$, $a_c = 255\,\mu$m (Table 1), yielding $b \approx 300.79\,\mu$m, and fluid shell thickness $\approx 45.79\,\mu$m.

Boundary conditions for the hemispheres-in-cell model include no-slip boundaries at grain surfaces, nontangential stress at the fluid envelope outer boundary, symmetry boundaries at the outer lateral cell boundaries, and stipulations on velocity (or pressure) at the cell entry and exit planes. Because the STAR-CD and Star-ccm+ software used in our simulations do not provide options to directly implement the nontangential stress condition on the fluid−fluid interface, this condition was implemented by adapting the boundary condition equation imposed on the outer fluid boundary of the Happel sphere-in-cell model to the Hemispheres-in-cell model, as described in the SI. The fluid flow field was developed via solution of the steady-state Navier−Stokes equation under laminar flow hydrodynamics, in conjunction with the continuity equation. Details on the resulting fluid flow field and estimation of pressure drop in the hemispheres-in-cell model are provided in the SI.

Particle Trajectory Analysis. A Lagrangian approach was used to mechanistically simulate particle trajectories based on the classical Langevin equation:

$$(m + m^*)\frac{\mathrm{d}u}{\mathrm{d}t} = F_\mathrm{D} + F_\mathrm{G} + F_\mathrm{L} + F_\mathrm{EDL} + F_\mathrm{vdW} + F_\mathrm{B} \tag{1}$$

where m is the particle mass, m^* is the virtual mass (approximated by one-half the displaced fluid volume by the particle) (*18*), u is the particle velocity vector, and the terms on the right-hand-side of the equation are the forces acting on the particle. These forces include fluid drag (F_D), gravity (F_G), shear lift (F_L), electrostatic (F_EDL), van der Waals (F_vdW), and Brownian forces (F_B), with expressions for these forces provided in Table 2. Among the forces, F_L, F_EDL, and F_vdW only act on the particle in the normal direction relative to the collector surface. Hydrodynamic retardation correction of the drag and Brownian forces (shown in Table 2) is described in the SI.

An adaptive time-stepping strategy was used in integrating all forces acting on the particle to obtain particle velocities according to eq 1. The constraints on the adaptive time-stepping strategy are described in the SI. Since the adaptive time-stepping strategy allows accounting for the rapid change of colloidal forces near a surface, first-order integration of the forces acting on the particles was implemented to determine the particle velocity according to eq 2. At each trajectory step, the integration was carried out in the normal and tangential direction relative to the collector surface respectively. The particle velocity vector (u_n, u_t) at time step τ was obtained from previous time step $\tau - 1$ as follows (derivation of these expressions is provided in the SI):

$$u_n^\tau = \frac{\left(m + \frac{2}{3}\pi a_\mathrm{p}^3\rho_\mathrm{f}\right)u_n^{\tau-1} + (F_n^\mathrm{GRP} + 6\pi\mu a_\mathrm{p} v_n f_2)\Delta t}{\left(m + \frac{2}{3}\pi a_\mathrm{p}^3\rho_\mathrm{f} + \frac{6\pi\mu a_\mathrm{p}}{f_1}\Delta t\right)}$$
$$u_t^\tau = \frac{\left(m + \frac{2}{3}\pi a_\mathrm{p}^3\rho_\mathrm{f}\right)u_t^{\tau-1} + \left(F_t^\mathrm{GRP} + \frac{f_3}{f_4}6\pi\mu a_\mathrm{p} v_t\right)\Delta t}{m + \frac{2}{3}\pi a_\mathrm{p}^3\rho_\mathrm{f} + \frac{1}{f_4}6\pi\mu a_\mathrm{p}\Delta t} \tag{2}$$

where $F_n^\mathrm{GRP} = F_\mathrm{G}{}^n + F_\mathrm{L} + F_\mathrm{EDL} + F_\mathrm{vdW} + F_\mathrm{B}{}^n$ and $F_t^\mathrm{GRP} = F_\mathrm{G}{}^t + F_\mathrm{B}{}^t$; the superscript and subscript n and t refer to the normal and tangential direction with respect to the collector surface respectively.

Upon resolving the particle velocity vector, the updated particle position was determined from first-order integration ($\mathrm{d}\mathbf{x}/\mathrm{d}t = u$), where $\mathbf{x}$ is the particle position vector. Following the trajectory step (translation), forces acting on the particle were determined, and the process was repeated until the particle exited, or was retained within the unit cell via attachment to the collector surface (defined as $h < 1$ nm), or remained within the cell without attachment despite the simulation time (2400 s) being twice the time of injection of the last colloid (1200 s).

Coupling Particle Trajectory Analysis to Computational Flow Field. Evaluating the forces acting on the particle required determining the fluid velocity vector at the particle location, which required determining the nearest computational mesh node to the particle. Due to the large number of mesh cells (more than 1 million), the computational expense of determining the closest mesh node to the colloid location needed to be minimized. To reduce computational expense, an array was created for each velocity node that listed the neighboring velocity nodes (nodes from adjacent face-sharing mesh cells). After introducing the colloid to a particular cell at the start of the simulation, the closest velocity node was determined from the set of nodes including the original node as well as all of its neighbors, as well as the neighbors of the neighbors, to ensure determination of the closest node in the polyhedral mesh. The distances between the colloid and the collector surfaces were computed by approximating the meshed surfaces with the ideal spherical surface. This was justified by the extremely fine discretization of the mesh at the grain surface. Simulations were performed in the presence of energy barriers to check whether slight nonparallel orientation of fluid velocity vectors (parallel to mesh elements) relative to the idealized spherical surface resulted in colloid attachment. The lack of colloid retention on the open grain surface in simulations in the presence of energy barriers indicates that approximating the mesh surface with an idealized sphere was reasonable.

The entry and exit planes to the hemispheres-in-cell model are located at the $z = -b$ and $z = b$ planes, respectively. At the entry plane, colloids were introduced via randomly chosen x and y coordinates ranging between $x = 0$ to a_c, and $y = -b$ to 0. Colloids initially located outside the fluid envelope were subject to fluid drag corresponding to the approach velocity. Once colloids entered into the fluid envelope, a complete force balance according to eq 1 was executed. Colloids that exit the fluid shell downstream of the grain-to-grain contact (i.e., $z > 0$) subsequently translated down-gradient via fluid drag (corresponding to the approach velocity) until they exited the system at the exit plane ($z = b$).

TABLE 2. Expressions for Forces Considered in the Langevin Equation

forces	expressions	references
electric double layer	$F_{EDL} = 4\pi\varepsilon_r\varepsilon_0\kappa a_p\zeta_p\zeta_c \times\left[\frac{\exp(-\kappa h)}{1+\exp(-\kappa h)} - \frac{(\zeta_p-\zeta_c)^2}{2\zeta_p\zeta_c}\frac{\exp(-2\kappa h)}{1-\exp(-2\kappa h)}\right]$	*23*
van der Waals	$F_{vdW} = -\frac{Ha_p\lambda(\lambda+22.232h)}{6h^2(\lambda+11.116h)^2}$	*24*
shear lift	$F_L = \frac{6.46\mu a_p^3(\partial v/\partial r)^{3/2}}{\nu^{0.5}}$	*25, 26*
Brownian	$F_B = \mathscr{R}\sqrt{\frac{2\xi kT}{\Delta t}}$	*27, 28*
drag (normal)	$F_D^n = -\frac{6\pi\mu a_p u_n}{f_1} + 6\pi\mu a_p v_n f_2$	*29, 30*
drag (tangential)	$F_D^t = -\frac{6\pi\mu a_p u_t}{f_4} + \frac{f_3}{f_4}6\pi\mu a_p v_t$	*31–33*
gravitational	$F_G = \frac{4}{3}\pi a_p^3(\rho_p-\rho_f)g$	–

$\varepsilon_r\varepsilon_0$ is the permittivity of water; κ is the reciprocal Debye length; ζ_p,ζ_c are the zeta potential of the particle and the collector respectively; h is the separation distance between the particle and the collector; λ is the characteristic wave length; μ and ν are the dynamic and kinematic viscosity of the fluid respectively; $\partial v/\partial r$ is the fluid velocity gradient normal to the collector surface; $\mathscr{R}$ is the Gaussian random number; ξ is the friction coefficient (equal to $6\pi\mu a_p$ in the bulk solution); k is the Boltzmann constant, and T is the absolute temperature; ρ_p and ρ_f are the density of the particle and the fluid respectively; f_1, f_2, f_3, and f_4 are universal hydrodynamic functions. The superscript and subscript n and t refer to the direction normal and tangential to the collector surface respectively.

Required Number of Trajectories. The probabilistic nature of Brownian forces requires that a sufficiently large population of colloid trajectories be simulated to determine a robust value for the collector efficiency. Simulations were performed under a range of fluid flow conditions representing ambient to forced-gradient groundwater flow, corresponding to average pore water velocities ranging from 4 to 400 m/day. Under the 4 m/day condition, a constant simulated value of η required 4000 particle trajectories; whereas, under the 40−400 m/day conditions, obtaining a constant value of η required between 10 000 and 40 000 trajectories.

Model Results and Discussion

Simulated Collector Efficiencies As Functions of Particle Size and Fluid Velocity. Simulated collector efficiencies from the hemispheres-in-cell geometry are shown as a function of particle size at three representative fluid velocities (Figure 2). For all conditions, the simulated collector efficiencies show a minimum value in colloid size range from 1 to 3 μm (specific minimum depending on fluid velocity), a trend that has been well established in previous models and experiments (*1–3, 8*). The simulated collector efficiency for a given particle size decreases with increasing fluid velocity, a trend that is also expected from previous models and experiments (*1–3, 8, 12, 20*). Variability in the simulated values of η decreases with increasing numbers of trajectories as described in the SI.

Simulated collector efficiencies from the Happel model via regression equations from Rajagopalan and Tien (*2, 21*) (RT) and Tufenkji and Elimelech (*3*) (TE) are shown (Figure 2). Note that as a result of subsequent clarifications to the RT equation, the RT equation refers to eq 4 in Nelson and Ginn (*1*) or eq 7.6 in Tien and Ramarao (*21*), and the TE equation refers to eq 17 in Tufenkji and Elimelech (*3*). Furthermore, the TE collector efficiency was normalized to the number of colloids flowing past the solid collector (as opposed to the solid collector plus the fluid shell); hence, in order to compare directly to the RT and the hemispheres-in-cell models, the η from the TE equation must be multiplied by γ^2, where $\gamma = (1-\varepsilon)^{1/3}$, as explained in Nelson and Ginn (*1*), and where ε is porosity. The comparison in Figure 2 shows good general agreement of the hemisphere-in-cell model with these two Happel-based models. Specifically, the hemisphere-in-cell collector efficiencies for the <1 μm particles (Brownian regime) match closely the TE results, but fall below the RT results, due to differences in treatment of hydrodynamic retardation and van der Waals interactions, as discussed in Tufenkji and Elimelech (*3*) and Nelson and Ginn (*1*). The convergence of results between the hemisphere-in-cell and TE (Happel sphere-in-cell) for <1 μm colloids suggests that the difference in these two model geometries

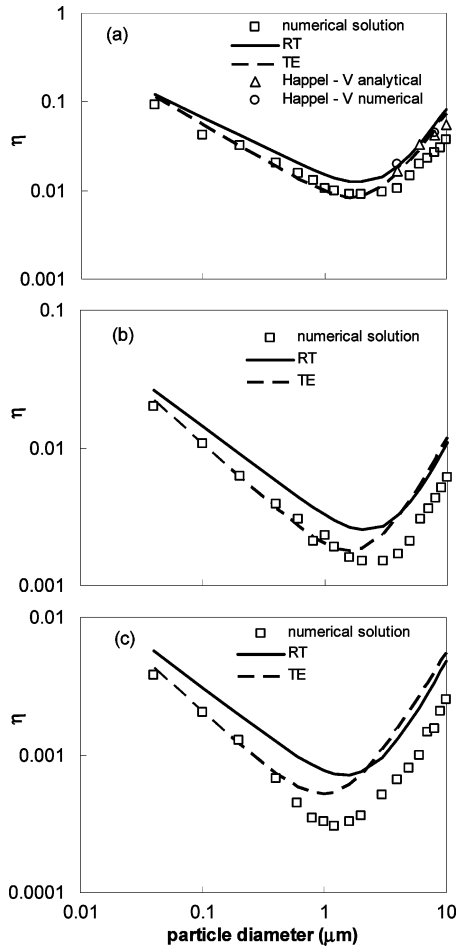

FIGURE 2. Comparison of simulated collector efficiencies (η, open squares) with the RT and TE predictions at three representative pore water velocities: (a) 4 m/day; (b) 40 m/day; and (c) 400 m/day. Values for other parameters are shown in Table 1. Also shown in panel (a) were simulated collector efficiencies from trajectory analyses on the Happel model for several larger particle sizes: (i) using the analytical flow field from Rajagopalan and Tien (*2*) (open triangles) and (ii) using the numerical flow field obtained from computational fluid dynamics (open circles).

produce negligible differences in colloid deposition (in the absence of energy barriers) for <1 μm colloids.

For larger particle sizes (e.g., >2 μm), the hemisphere-in-cell collector efficiencies were significantly lower (~a factor of 2) than both the RT and TE results (Figure 2), suggesting that differences in the hemisphere-in-cell versus Happel sphere-in-cell geometries (presence versus absence of grain-to-grain contact) slightly influenced collector efficiencies in the absence of energy barriers. Alternatively, this difference may reflect (i) errors in our particle trajectory analysis; (ii) the use of a computational flow field.

Validation of Particle Trajectory Analysis and Numerical Flow Field. To examine the influence of our particle trajectory simulations, we coupled our trajectory analyses with the Happel sphere-in-cell analytical flow field (*2*). The simulated values of η agreed well with the RT and TE predictions (Figure 2a), with very slight differences in η for the largest particles (8 and 10 μm), indicating that our particle trajectory analyses were not responsible for differences observed in Figure 2.

To examine the influence of the computational flow field, we constructed computational meshes for the Happel sphere-in-cell geometry and numerically solved the flow field under the above-mentioned boundary conditions. The simulated values of η based on our particle trajectory analyses coupled to the Happel cell computational flow field also agreed well with the RT and TE results (Figure 2a), demonstrating that the differences observed in Figure 2 were not caused by utilization of a computational flow field for the hemisphere-in-cell predictions. Hence, the prediction of lower collector efficiencies (for >2 μm colloids) by the hemisphere-in-cell model relative to the Happel-based models is due to differences in model geometries, which may result from (i) decreased projected area of the entry plane in the hemisphere-in-cell relative to Happel sphere-in-cell geometry; and (ii) divergent stream lines at the grain-to-grain contact in the hemisphere-in-cell (SI Figure S3). The average pore water velocity inside the hemispheres-in-cell collector was approximately a factor of 1.3 higher than that inside the Happel sphere-in-cell collector (at approach velocity of 1.48 m/day) as a result of the streamline divergence. This, coupled with the expected decrease in η with increasing fluid velocity (Figure 2), may produce the observed lower ηs for larger particle sizes observed in the hemisphere-in-cell results relative to the RT and TE Happel-based results.

TABLE 3. List of Dimensionless Parameters in Predicting Colloid Filtration

parameter	definition	description
N_R	d_p/d_c	aspect ratio
N_{PE}	Ud_c/D_{BM}	Peclet number
N_A	$H/(12\pi\mu a_p^2 U)$	attraction number
N_G	$2a_p^2(\rho_p-\rho_f)g/(9\mu U)$	gravity number

[a] d_p is the particle diameter; D_{BM} is the bulk diffusion coefficient (described by Stokes–Einstein equation); a_p is the particle radius; g is the gravitational acceleration constant; all the other parameters are defined in Table 1.

Correlation Equation for η Based on the Hemispheres-in-Cell Model. Colloid deposition predictions from the Happel sphere-in-cell geometry have been made widely available via correlation equations regressed to the mechanistic numerical results. As described above, two widely used correlation equations are the RT (*2*) and TE (*3*) equations. These models provide excellent prediction of particle deposition in simple porous media under favorable conditions (absent an energy barrier). We herein provide a correlation equation for the hemisphere-in-cell geometry; however, we stress that the purpose of providing this correlation equation for η is not to improve prediction of colloid deposition under favorable conditions in simple porous media (for which the existing equations are adequate), but rather to examine a new geometric model (the hemispheres-in-cell) by comparing its performance to existing models under favorable conditions and to distribute these results with the intention of laying a foundation for prediction of colloid retention under unfavorable conditions (in the presence of energy barriers).

Following the strategy described in the SI, individual components that contribute to η (i.e., η_I, η_G, and η_D, due to interception, sedimentation, and diffusion mechanism respectively) were simulated as a function of particle size at an average pore water velocity of 4 m/day, and the coefficients and exponents of the dimensionless parameters (Table 3) were then adjusted to fit the trends for η_I, η_G, and η_D. The overall resulting correlation equation for η in the hemispheres-in-cell geometry in the absence of energy barriers to deposition is

$$\eta \approx \gamma^2[2.3A_s^{1/3}N_R^{-0.080}N_{PE}^{-0.65}N_A^{0.052} + 0.55A_sN_R^{1.8}N_A^{0.15} + 0.2N_R^{-0.10}N_G^{1.1}N_A^{0.053}N_{PE}^{0.053}] \quad (3)$$

where the dimensionless parameters (i.e., N_R, N_{PE}, N_A, N_G) are defined in Table 3, and A_s is a porosity-dependent parameter defined as:

$$A_s = \frac{2(1-\gamma^5)}{2-3\gamma+3\gamma^5-2\gamma^6} \quad (4)$$

where $\gamma = (1-\varepsilon)^{1/3}$. It is worth mentioning that A_s accounts for influence of neighboring collectors on the fluid flow field in the Happel sphere-in-cell geometry. The lack of an analytical solution to the flow field in the hemisphere-in-cell geometry precludes development of the corresponding expression specific to that geometry. However, we adopt this parameter directly from the Happel sphere-in-cell geometry with the expectation that the dependence of flow field geometry on porosity encapsulated in A_s is similar in both the Happel and hemisphere systems. The excellent agreement of the correlation equation and the numerical simulations across a wide range of particle sizes and fluid velocities (Figure 3) indicates that this expectation is met. The correlation equation (i.e., eq 3) very slightly underestimates deposition of 1 μm colloids at the low fluid velocity (4 m/day); whereas, the equation very slightly overestimates deposition of 1 μm colloids at the high fluid velocity (400 m/day) (Figure 3). Comparison of predictions from the hemisphere-in-cell correlation equation with numerical simulations was also made for various porosity values, as described in a companion paper (*22*). This comparison demonstrated that the correlation equation matched numerical simulations closely across a large range of porosities.

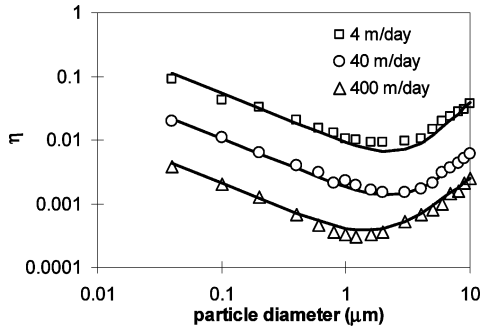

FIGURE 3. Comparison of predicted collector efficiencies from eq 3 (solid lines) with numerical simulation results from the hemispheres-in-cell model at three representative pore water velocities: □, 4 m/day; ○, 40 m/day; Δ, 400 m/day. Values for other parameters are shown in Table 1.

The hemispheres-in-cell correlation equation relates to previous correlation equations in the following ways: (i) The diffusion term (first term in bracket in eq 3) is nearly equivalent to that in the TE equation, and our numerical results in the Brownian regime (colloids < ~1 μm) closely match those of the TE (*3*). (ii) The insensitivity of the gravitational contribution to the numerical results to porosity (also observed by Tufenkji and Elimelech (*3*)) suggests that A_s should not be included in the sedimentation term (third term in bracket). (iii) Our simulations concerned a single Hamaker constant (i.e., 3.84×10^{-21} J), therefore we adopted the exponent for N_{vdW} ($=H/kT$) provided in the TE equation (*3*) and slightly modified it by observing that $N_{vdW} = N_A \times N_{PE}$. Note, the correlation is insensitive to this parameter, e.g., for our simulations, negligible changes occurred with versus without inclusion of N_{vdW} (replaced with $N_A \times N_{PE}$) in the first and third terms in eq 3.

Comparison with Experimental Data. Simulation of colloidal transport at the macroscale typically involves a deposition rate coefficient (k_f), which is obtained via a geometric relationship with the collector efficiency (η). Although η is dependent upon the specific geometry of unit collector, k_f is not. The following relationship between k_f and η for the hemispheres-in-cell geometry was developed following the analyses of Logan et al. (*19*) and Nelson and Ginn (*1*), as described in the SI:

$$k_f = \frac{3(1-\varepsilon)}{2d_c}\eta v_p\left[\frac{3-\varepsilon}{3-3\varepsilon} - \frac{2(3-\varepsilon)}{\pi(3-3\varepsilon)}\cos^{-1}\left(\frac{3-3\varepsilon}{3-\varepsilon}\right)^{1/2} + \frac{2}{\pi}\sqrt{2\left(\frac{3-\varepsilon}{3-3\varepsilon}\right)^{1/2}-1}\right] \quad (5)$$

where v_p is the average pore water velocity in the unit collector and d_c is the collector diameter. The deposition rate coefficient relationship with η for the Happel sphere-in-cell model is

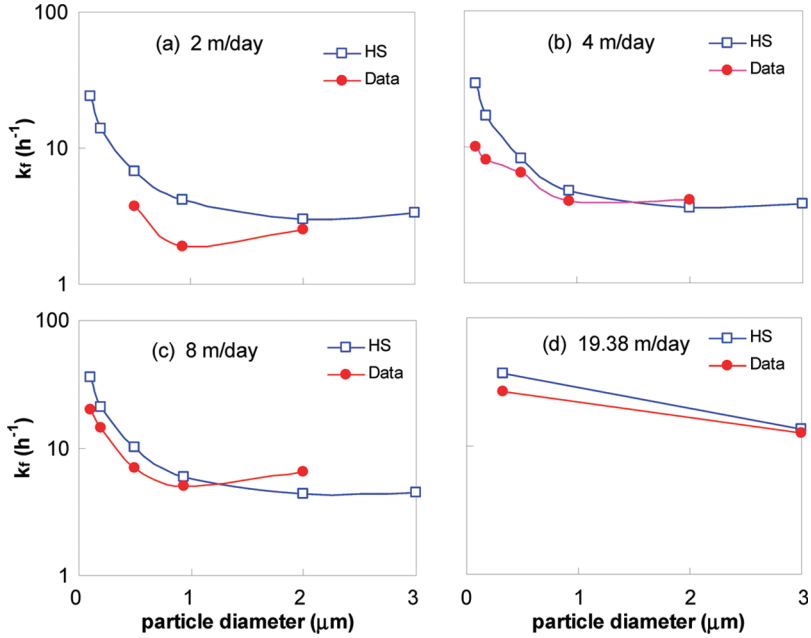

FIGURE 4. Simulated (blue open symbols) and observed (red closed symbols *8, 20*) deposition rate coefficients (k_f) in the absence of an energy barrier to deposition as a function of particle size at four fluid velocities: (a) 2 m/day; (b) 4 m/day; (c) 8 m/day; and (d) 19.38 m/day. Simulated deposition rate coefficients were calculated from eq 5 based on the hemispheres-in-cell model; and were slightly higher than corresponding observed deposition rate coefficients.

$$k_f = \frac{3(1-\varepsilon)^{1/3}}{2d_c}\eta v_p \quad (6)$$

where η in the equation above incorporates the term $(1-\varepsilon)^{2/3}$, as explained in Nelson and Ginn (*1*).

Values of k_f from the hemispheres-in-cell model (via eqs 3 and 5) were compared to experimentally measured k_f values in column experiments under equivalent conditions (Figure 4 and SI Table S2). The hemispheres-in-cell values for k_f matched very closely with experimentally observed k_f values, within a factor of ~2. The demonstrated agreement with existing theory and experiment under favorable conditions indicates that the hemispheres-in-cell model serves well as a new geometry that is capable of predicting colloid transport and retention in the absence, and potentially presence, of energy barriers. We stress here that our goal is not to improve prediction of colloid retention in porous media under favorable conditions; rather, our goal is to present this hemispheres-in-cell geometry that may potentially be used to predict colloid retention under unfavorable conditions (in the presence of energy barriers). In a subsequent paper we will examine the ability of the hemispheres-in-cell model to predict retention when energy barriers to deposition are present.

Acknowledgments

This article is based upon work supported by the National Science Foundation Chemical, Biological, and Environmental Transport, and Hydrologic Science Programs (0822102) and the U.S. Department of Agriculture grant 2006-02541. Any opinions, findings, and conclusions or recommendations expressed in this material are those of the authors and do not necessarily reflect the views of the National Science Foundation or the Department of Agriculture. We are grateful for the technical and facility support provided at the Center for High Performance Computing at the University of Utah. We thank Professor Chi Tien for his valuable suggestions and inputs on clarification of particle deposition processes. We also thank Professors Anthony Ladd and Jason Bulter for their useful discussion on representing Brownian motions in our trajectory analysis model. We are thankful for the three anonymous reviewers' comments that have greatly helped to improve this manuscript.

Supporting Information Available

Additional information, equations, Tables S1 and S2, and Figures S1−S4. This material is available free of charge via the Internet at http://pubs.acs.org.

Literature Cited

(1) Nelson, K. E.; Ginn, T. R. Colloid filtration theory and the happel sphere-in-cell model revisited with direct numerical simulation of colloids. *Langmuir* **2005**, *21* (6), 2173–2184.
(2) Rajagopalan, R.; Tien, C. Trajectory analysis of deep-bed filtration with the sphere-in-cell porous media mODEL. *AIChE J.* **1976**, *22* (3), 523–533.
(3) Tufenkji, N.; Elimelech, M. Correlation equation for predicting single-collector efficiency in physicochemical filtration in saturated porous media. *Environ. Sci. Technol.* **2004**, *38* (2), 529–536.
(4) Yao, K.-M.; Habibian, M. T.; O'Melia, C. R. Water and waste water filtration: Concepts and applications. *Environ. Sci. Technol.* **1971**, *5* (11), 1105–1112.
(5) Happel, J. Viscous flow in multiparticle systems: Slow motion of fluids relative to beds of spherical particles. *AIChE J.* **1958**, *4* (2), 197–201.
(6) Adamczyk, Z.; Dabros, T.; Czarnecki, J.; van de Ven, T. G. M. Particle transfer to solid surfaces. *Adv. Colloid Interface Sci.* **1983**, *19* (3), 183–252.
(7) Elimelech, M.; O'Melia, C. R. Kinetics of deposition of colloidal particles in porous media. *Environ. Sci. Technol.* **1990**, *24* (10), 1528–1536.
(8) Tong, M.; Johnson, W. P. Excess colloid retention in porous media as a function of colloid size, fluid velocity, and grain angularity. *Environ. Sci. Technol.* **2006**, *40* (24), 7725–7731.
(9) Shellenberger, K.; Logan, B. E. Effect of molecular scale roughness of glass beads on colloidal and bacterial deposition. *Environ. Sci. Technol.* **2002**, *36* (2), 184–189.
(10) Song, L.; Johnson, P. R.; Elimelech, M. Kinetics of colloid deposition onto heterogeneously charged surfaces in porous media. *Environ. Sci. Technol.* **1994**, *28* (6), 1164–1171.
(11) Johnson, W. P.; Li, X.; Yal, G. Colloid retention in porous media: Mechanistic confirmation of wedging and retention in zones of flow stagnation. *Environ. Sci. Technol.* **2007**, *41* (4), 1279–1287.
(12) Li, X.; Lin, C.-L.; Miller, I. D.; Johnson, W. P. Pore-scale observation of microsphere deposition at grain-to-grain contacts over assemblage-scale porous media domains using x-ray microtomography. *Environ. Sci. Technol.* **2006**, *40* (12), 3762–3768.
(13) Bradford, S. A.; Simunek, J.; Bettahar, M.; Van Genuchten, M. T.; Yates, S. R. Modeling colloid attachment, straining, and exclusion in saturated porous media. *Environ. Sci. Technol.* **2003**, *37* (10), 2242–2250.
(14) Hahn, M. W.; O'Melia, C. R. Deposition and reentrainment of Brownian particles in porous media under unfavorable chemical conditions: Some concepts and applications. *Environ. Sci. Technol.* **2004**, *38* (1), 210–220.
(15) Redman, J. A.; Walker, S. L.; Elimelech, M. Bacterial adhesion and transport in porous media: Role of the secondary energy minimum. *Environ. Sci. Technol.* **2004**, *38* (6), 1777–1785.
(16) Cushing, R. S.; Lawler, D. F. Depth filtration: Fundamental investigation through three dimensional trajectory analysis. *Environ. Sci. Technol.* **1998**, *32* (23), 3793–3801.
(17) STAR-CD and Star-ccm+ software packages developed by CD-Adapco. www.cd-adapco.com.
(18) Gondret, P.; Lance, M.; Petit, L. Bouncing motion of spherical particles in fluids. *Phys. Fluids* **2002**, *14*, 643–652.
(19) Logan, B. E.; Jewett, D. G.; Arnold, R. G.; Bouwer, E. J.; O'Melia, C. R. Clarification of clean-bed filtration models. *J. Environ. Eng.* **1995**, *121* (12), 869–873.
(20) Tufenkji, N.; Elimelech, M. Breakdown of colloid filtration theory: Role of the secondary energy minimum and surface charge heterogeneities. *Langmuir* **2005**, *21* (3), 841–852.
(21) Tien, C.; Ramarao, B. V. *Granular filtration of aerosols and hydrosols*; Elsevier: Oxford, 2007.
(22) Ma, H.; Johnson, W. P. Colloid retention in porous media of various porosities: Predictions by the hemispheres-in-cell model. *Langmuir* **2009**, DOI: 10.1021/la902657v.
(23) Hogg, R.; Healy, T. W.; Fuerstenau, D. W. Mutual coagulation of colloidal dispersions. *Trans. Faraday Soc.* **1966**, *62*, 1638–1651.
(24) Elimelech, M.; Gregory, J.; Jia, X.; Williams, R. A. *Particle Deposition & Aggregation: Measurement, Modeling and Simulation*; Butterworth: Boston, 1995.
(25) Saffman, P. G. The lift on a small sphere in a slow shear flow. *J. Fluid Mech.* **1965**, *22* (2), 385–400.
(26) Saffman, P. G. Corrigendum on "The lift on a small sphere in a slow shear flow". *J. Fluid Mech.* **1968**, *31*, 624.
(27) Kubo, R. The fluctuation-dissipation theorem. *Rep. Prog. Phys.* **1966**, *29,* 255–284.
(28) Ounis, H.; Ahmadi, G.; McLaughlin, J. B. Brownian diffusion of submicrometer particles in the viscous sublayer. *J. Colloid Interface Sci.* **1991**, *143* (1), 266–277.
(29) Brenner, H. The slow motion of a sphere through a viscous fluid towards a plane surface. *Chem. Eng. Sci.* **1961**, *16*, 242–251.
(30) Goren, S. I.; O'Neill, M. E. On the hydrodynamic resistance to a particle of a dilute suspension when in the neighborhood of a large obstacle. *Chem. Eng. Sci.* **1971**, *26* (3), 325–338.
(31) Goldman, A. J.; Cox, R. G.; Brenner, H. Slow viscous motion of a sphere parallel to a plane wall—I Motion through a quiescent fluid. *Chem. Eng. Sci.* **1967**, *22*, 637–651.
(32) Goldman, A. J.; Cox, R. G.; Brenner, H. Slow viscous motion of a sphere parallel to a plane wall—II Couette flow. *Chem. Eng. Sci.* **1967**, *22*, 653–660.
(33) Spielman, L. A.; CUKor, P. M. Deposition of non-Brownian particles under colloidal forces. *J. Colloid Interface Sci.* **1973**, *43* (1), 51–65.

ES901242B